JOURNAL OF MATERIALS SCIENCE 23 (1988) 2521–2532

Ductile-to-brittle transition of rubber-modified polypropylene

Part 1 *Irreversible deformation mechanisms*

C. J. CHOU*, K. VIJAYAN‡, D. KIRBY§, A. HILTNER, E. BAER
Center for Applied Polymer Research, Department of Macromolecular Science, Case Western Reserve University, Cleveland, Ohio 44106, USA

The irreversible deformation mechanisms of polypropylene (PP) blended with an ethylene–propylene rubber (EPR) were investigated in the region of the ductile-to-brittle (D-B) transition. The nature of the D-B transition over the composition range of 0 to 25% EPR was studied as a function of temperature and strain rate. Optical microscopy and scanning electron microscopy were used to examine the irreversible microdeformation processes in the fractured specimens. At −40° C, the controlling irreversible deformation process in PP was crazing. In the blends, two kinds of damage zones were observed: a diffuse zone due to voiding at rubber particles and an intense damage zone due to craze-like damage and deformation bands. In general, the size and density of the damage zones increase in a gradual manner through the D-B transition whether examined as a function of temperature, strain rate or blend composition.

1. Introduction

The enhancement of the impact properties of polypropylene (PP) by introduction of a rubbery phase is a well-known phenomenon that is widely utilized commercially. In particular, melt-blending of PP with various rubbers such as ethylene–propylene rubber (EPR), ethylene–propylene–diene terpolymer (EPDM), and styrene–butadiene–styrene block copolymer (SBS) has been used. The effects of these impact modifiers on the morphological characteristics of PP have been extensively investigated [1–8]. The spherulite size, nucleation and growth rate of PP are all affected by these impact modifiers. Furthermore, it is known that, in these blends, rubber particles narrowly distributed around 0.5 to 1 μm in size are the most effective for toughening PP [8].

The impact properties of rubber-modified PP have been investigated by a variety of techniques [9–15]. Blend composition as well as the processing conditions used in preparation of the blend are important variables that influence the impact behaviour. A very striking characteristic of the deformation of modified PP is stress-whitening. The dilational deformation mechanisms that produce stress-whitening may include both crazing and void formation [16, 17]. Crazing associated with rubber particles in impact-modified PP has been observed in the transmission electron microscope [18–20]. Microvoiding at the rubber–matrix interface has been recently observed [21]. Matrix yielding is another important deformation mechanism in rubber-modified PP recognized by many investigators [18–22]. Although the irreversible deformation mechanisms in rubber-modified PP have been identified by these authors, a systematic study of how these mechanisms change during the transitional behaviour from ductile to brittle has not been reported. For this purpose, the microdeformation processes of PP–EPR blends have been investigated in the ductile-to-brittle transition region as a function of temperature, strain rate and blend composition.

2. Experimental procedure

2.1. Materials

Blends were prepared from Hercules Profax 6523 (Hercules Inc., Wilmington, DE 19894) polypropylene (PP) and Exxon Vistalon PA714 (Exxon Chemical Co., Houston, TX 77001) ethylene–propylene copolymer (EPR). Pellets of the two polymers were dry-blended to PP, EPR compositions of 95/5, 90/10, 85/15, 80/20, and 75/25 by weight, and melt-blended in a single-screw Newberry injection-moulding machine at 300 p.s.i. (2.07 MPa) hydraulic back-pressure. The melt mixtures were injection-moulded into plaques (100 mm × 100 mm × 3.3 mm) and rectangular bars (120 mm × 12 mm × 3 mm). Specimens for low-speed tensile tests were machined from the plaques according to ASTM specification D 638 Type 4. These specimens had a skin layer about 0.1 mm thick that was removed by machining 0.5 mm from both sides of the specimens. Rectangular specimens (40 mm × 12 mm × 3 mm) for high-speed tensile tests were cut from the bars. A 45° blunt notch 4 mm in depth was machined at the centre of each specimen.

2.2. Mechanical measurements

Tensile tests were carried out at a strain rate

* *Present address*: Dow Chemical Company, Freeport, TX 77541, USA.
‡ *Present address*: Richards Medical Company, Memphis, TN 38116, USA.
§ Whirlpool Corporation, Benton Harbour, Michigan 49022, USA.

0022–2461/88 $03.00 + .12

1.4% min^{-1} on an Instron testing machine using an environmental chamber cooled by vaporized liquid carbon dioxide; the temperature was controlled to an accuracy of $\pm 1°C$. Elastic moduli were measured at a strain rate of 0.3% min^{-1} with an Instron strain-gauge extensometer. The moduli were calculated at 1% elongation. High-speed tensile tests were run on an MTS servohydraulic testing machine at room temperature. Impact strength was measured on sheets (100 mm × 100 mm × 3.3 mm) with a Dynatup instrumented drop-dart at ambient temperature. The drop rate was 4.20 m sec^{-1}.

2.3. Microscopy

An Olympus microscope was used for the optical micrographs. The spherulitic structure of the bulk was determined from thin sections about 10 μm thick taken from the core region of the sample. The specimens were microtomed with fresh glass knives at room temperature. Spherulite growth rates were studied in the polarizing optical microscope equipped with a hot stage. The specimens were heated to 200° C for 5 min, then crystallized isothermally at the desired temperature. The spherulite growth rate was subsequently determined from micrographs taken at appropriate time intervals.

Fractured specimens were embedded in clear epoxy and then ground and polished on both faces to produce thin sections from the core region of the specimen about 20 to 40 μm in thickness.

Rubber particle size and distribution in the blend were examined in a Jeol 35 CF scanning electron microscope (SEM). Samples were first immersed in liquid nitrogen for 30 min, and were microtomed with glass knives immediately after removal from liquid nitrogen. The specimens were then immersed in xylene in an ultrasonic bath at room temperature for 9 min to dissolve rubber particles at the surface. After etching, the specimens were removed from xylene and air-dried. The specimens were coated with gold–palladium alloy before examination in the SEM.

Fracture surfaces were also examined by SEM after coating with gold–palladium alloy. Before coating, some of the fracture surfaces were etched with xylene using the procedure described above.

2.4. Calorimetry measurements

The thermal properties of the blends were studied with a Perkin–Elmer differential scanning calorimeter (DSC) Type 2 at a heating rate of 10° C min^{-1}. The glass transition temperature of PP and the melting temperatures and enthalpies of PP and EPR were obtained from the thermograms.

3. Results and discussion

3.1. Blend morphology

The thermal properties of polypropylene and EPR resins and their injection-moulded blends are summarized in Table I. The glass transition temperature of PP is observed at about 0° C in both the resin and the rubber-modified blends. The crystalline melting temperatures, taken from the peaks in the DSC thermograms, are about 165° C for PP and 127° C for EPR, and the melting peaks of both components are observed in the thermograms of the blends at about the same temperatures as the resins. The heats of melting of PP and EPR in all the compositions, normalized to the amount of resin in the sample, are about 84 and 54 J g^{-1}, respectively. This is consistent with a previous report that the heat of melting per unit of PP in PP blends is independent of the rubber content of the blend [4]. Based on the literature values for the heat of fusion of PP and polyethylene [23], the degree of crystallinity of PP and EPR in all the compositions is estimated to be about 40 and 23%, respectively. From the thermal measurements, PP and EPR form immiscible, phase-separated blends with the additional feature that the crystallinity and crystalline melting point of both phases are essentially unaffected by the presence of the second phase. Since the melting behaviour in the DSC is determined primarily by the characteristics of crystallites, this latter feature suggests that the crystalline structure of PP at the size scale of the lamellae is not strongly affected by the presence of an EPR phase.

While the EPR phase does not affect the crystallinity of PP, the spherulite morphology as seen in optical micrographs of thin sections cut from the injection-moulded plaques is altered. The average spherulite size of PP (Table I) decreases by almost a factor of 2 from 90 μm in PP resin to 50 μm in the 5% rubber blend. In addition, the sharp interspherulite boundaries that characterize PP (Fig. 1) are not evident in the blends, where by comparison the boundaries are irregular and difficult to distinguish in the micrographs. The spherulites gradually become smaller and more irregular in shape as the rubber content increases, for example the average spherulite size decreases from 50 to 40 μm as the rubber content is increased from 5 to 20%. Nevertheless, these changes

TABLE I Characterization of polypropylene blends

Sample PP (%)	Heat of Melting (J g^{-1})*		T_m (° C)		T_g (° C)	Average PP spherulite size (μm)
	PP	EPR	PP	EPR	PP	
100	83.0	-	165	-	−4	90
95	86.3	44.8	166	126	1	50
90	85.1	56.6	165	127	−2	45
85	83.0	59.9	164	127	−1	40
80	83.8	64.5	166	127	−2	40
75	82.5	48.2	165	127	−1	40
0	-	51.1	-	126	-	-

*Normalized with sample weight.

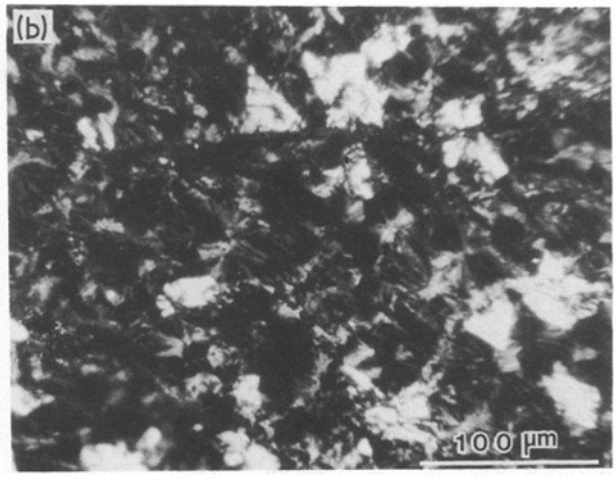

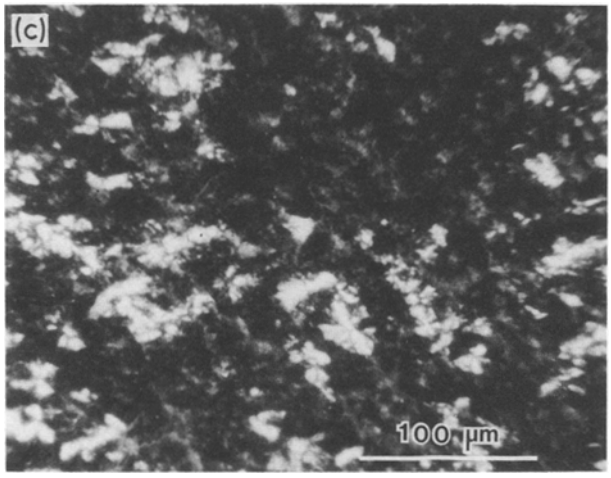

Figure 1 Optical micrographs of microtomed sections from injection-moulded plaques of (a) PP, (b) 95% PP–5% EPR, (c) 75% PP–25% EPR.

in spherulite morphology, which have also been observed in other blends of PP and appear to be a general effect [2, 3, 7], are most pronounced when the first 5% rubber is added and further changes in morphology are small when the rubber content is increased further.

The rubber phase that is not distinguishable in the optical microscope in sections cut from plaques such as those in Fig. 1 becomes visible when the section is melted on the hot stage of the microscope and allowed to recrystallize as a very thin film. Comparison of the spherulitic structures of PP and a blend with 15% rubber grown at 131°C in Fig. 2 shows the rubber dispersed throughout the spherulite as spherical particles on the size scale of 1 to 2 μm in diameter. Increasing the rubber content changes only the density of rubber particles, not the size or shape. Some coalescence of the rubber particles into larger irregularly shaped domains occurs only at a higher isothermal crystallization temperature, 141°C, where the growth rate is very slow.

Dependence of the isothermal spherulite growth rate on blend composition at two temperatures is shown in Table II. The data are consistent with reports in the literature on similar blends of PP [4, 5] and show that the rate of about 10 μm min^{-1} in diameter at the higher temperature is independent of composition; while at the lower temperature, where the growth rate is about 35 μm min^{-1}, there may be a small drop in the growth rate for the blends. While incorporation of the elastomer does not strongly affect the growth rate, it is known that nucleation of PP spherulites occurs more rapidly when a rubber phase is present [4, 5]. Probably, this effect is responsible for the smaller spherulite size in the blends.

The size and distribution of rubber particles in the injection-moulded plaques are clearly seen when etched specimens are viewed in the SEM (Fig. 3). Spherical depressions about 1 μm in diameter remain where the rubber was etched away by the solvent. An increase in the amount of rubber produces a higher density of

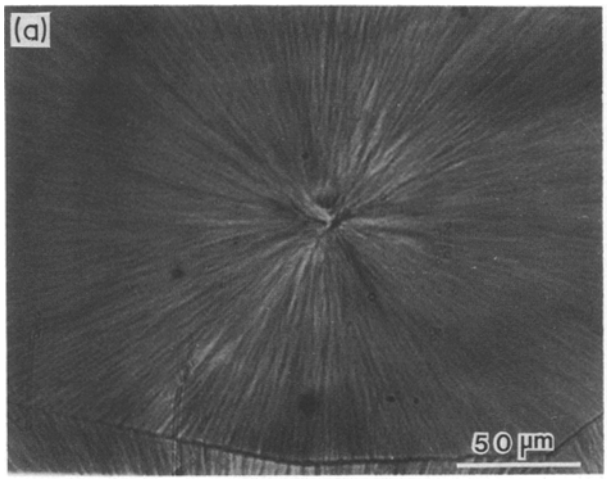

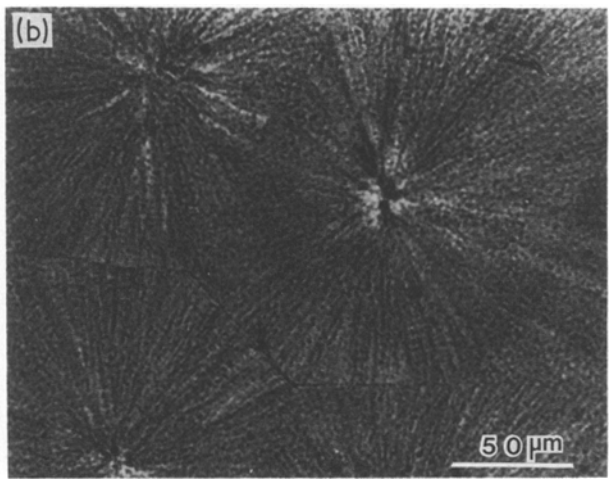

Figure 2 Optical micrographs of thin films crystallized from the melt at 131°C: (a) PP, (b) 85% PP–15% EPR.

TABLE II Spherulite growth rate of PP in the PP blends at two crystallization temperatures

Sample PP (%)	Growth rate ($\mu m\,min^{-1}$)	
	131° C	125° C
100	11	37
95	10	33
90	11	35
85	10	40
80	10	30
75	10	33

depressions but no significant change in their size. The depressions are uniformly distributed in the micrograph over a viewing area that is comparable to the size of a spherulite, 40 to 50 μm. The morphologies of injection-moulded and isothermally crystallized blends are analogous in that the rubber phase is dispersed as 1 μm particles uniformly distributed through the spherulites of PP. The intraspherulitic regions occupied by rubber particles are probably the amorphous regions between lamallae, since the melting behaviour of the blends is essentially the same as that of the unmodified resins.

3.2. Deformation at low temperatures

The first method by which the ductile-to-brittle transition was studied utilized tensile deformation of unnotched specimens at low temperatures. When unnotched specimens of PP and its blends with EPR were drawn in tension with the temperature variable, the glass transition was accompanied by a change in the deformation mode from neck formation and cold drawing to uniform deformation of the entire gauge section. It was found that effects of blend composition were most apparent below the glass transition temperature where uniform deformation rather than necking was observed.

The stress–strain curves of a blend with 10% EPR at three temperatures below the glass transition temperature are shown in Fig. 4. At all temperatures, stress-whitening preceded fracture, and the arrows

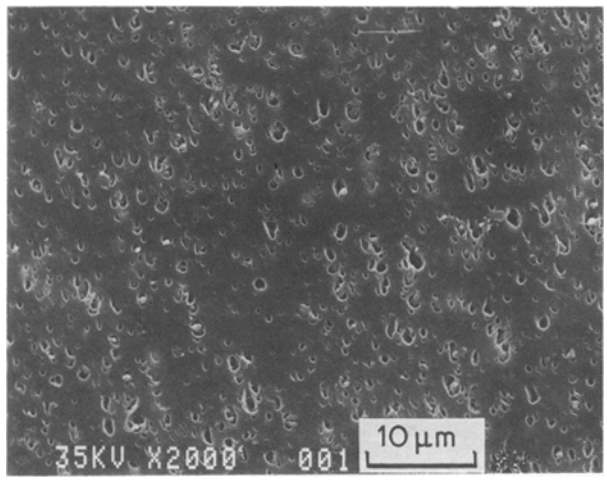

Figure 3 Scanning electron micrographs of the xylene-etched microtomed surface of 85% PP–15% EPR blend.

indicate the stresses at which stress-whitening was first visible. These are close to but slightly higher than the onset of non-linearity in the stress–strain curve. Both the stress at the onset of stress-whitening and the maximum stress increased as the temperature decreased. A ductile-to-brittle transition can be defined from the shape of the stress–strain curves, where a brittle specimen is one that breaks at the maximum stress, and a ductile specimen is one for which the stress falls below the maximum before fracture. By this definition, a ductile-to-brittle transition occurs in the 10% EPR blend between $-40°$ C and $-60°$ C.

The effect of increasing EPR in the blend composition was analogous to increasing the temperature (Fig. 5). At $-40°$ C, the shape of the stress–strain curve shows a ductile-to-brittle transition between 10 and 5% EPR. The arrows on the stress–strain curves indicate the stresses at which stress-whitening was first observed visually. The modulus (Table III), stress at onset of observable irreversible deformation and maximum stress all decreased as the rubber content increased. In PP, the stress-whitening was

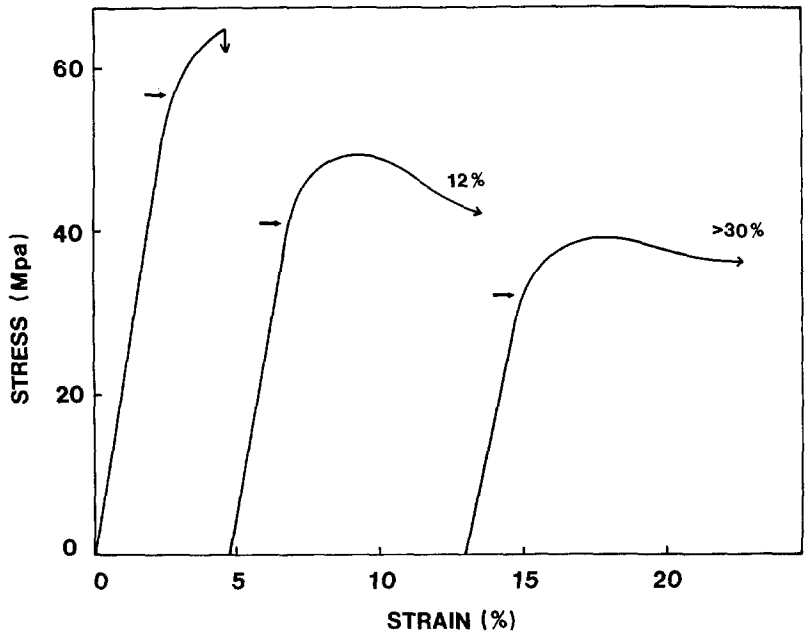

Figure 4 Tensile stress–strain curves of 90% PP–10% EPR at three temperatures.

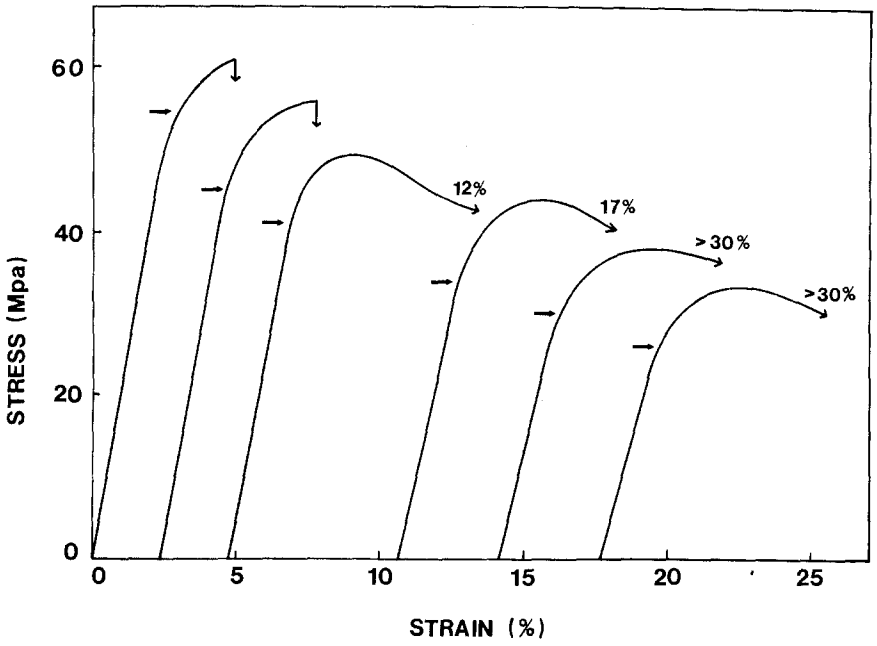

Figure 5 Tensile stress–strain curves of PP blends at −40° C.

concentrated along lines perpendicular to the applied stress. In the blends, more diffuse whitening was observed first in a small region of the specimen and then spreading to the entire gauge length before the maximum stress was attained. Polypropylene and the blend with 5% EPR fractured catastrophically at the maximum stress at strains of about 5 and 7%, respectively. Blends with 10 and 15% EPR failed after the maximum stress with elongations at break of about 12 and 17%, respectively. In both compositions, crack initiation occurred in a region of intense stress-whitening at the maximum stress. The crack propagated slowly to a length of about 0.5 mm in the 10% EPR specimen before the specimen fractured catastrophically. In comparison, the crack was blunted in the 15% EPR and followed a slow tearing mode of propagation across the entire width of the specimen. Blends with 20 and 25% EPR showed uniform extension of the entirely stress-whitened specimen and no visible crack initiation after 30% elongation.

Longitudinal sections cut from the fractured specimens were examined in the optical microscope in order to observe the damage processes that give rise to macroscopic stress-whitening. Regions close to the fracture site are shown in Fig. 6. Since the strain prior to fracture was increasing as rubber content increased, irreversible deformation is more extensive in the higher-rubber blends. In unmodified PP resin, craze-like damage perpendicular to the applied stress is similar to that observed by others [24, 25]. The craze density is highest near the fracture site and decreases away from the fracture site. The length of the crazes varies from 50 μm to several millimetres. The lines parallel to the direction of the applied stress are polishing lines. More dense craze-like damage is observed in the 5% EPR blend shown in Fig. 6b. These crazes are shorter than in PP and not as well aligned perpendicular to the applied stress. As the amount of deformation prior to fracture increases with 10% EPR (Fig. 6c) the crazes begin to intersect each other at an angle of about 30 to 40°, particularly near the fracture site. In blends with 15% EPR (Fig. 6d) and higher, the damage resembles a network of crossing deformation bands that covers the entire specimen.

TABLE III Modulus of PP blends at −40° C

Sample PP (%)	Modulus (GPa)
100	4.01
95	3.84
90	4.18 (−60° C)
	3.65 (−40° C)
	3.33 (−20° C)
85	3.40
80	3.22
75	3.06

Fracture surfaces of the specimens from the stress–strain experiments at −40° C are shown in Fig. 7 as viewed in the SEM. The low magnification shows the entirely brittle fracture surface of PP. The fracture surfaces of blends with 10 and 5% EPR are characteristic of mixed-mode fracture with a smooth region of ductile fracture together with a region of brittle fracture. The blend with 15% EPR shows an entirely ductile fracture surface with sucking-in of the sides and a tearing line along the centre of the fracture surface. Microscopic observations of irreversible deformation prior to fracture in all specimens with progressive changes in intensity of the damage, and analysis of mixed-mode fracture surfaces, demonstrate that the ductile-to-brittle transition is gradual and a definition based on the shape of the stress–strain curve is overly simplified. Nevertheless, when comparisons are made and the transitional compositions of 5 and 10% EPR in the stress–strain curves are found to be those that exhibit mixed-mode fracture surfaces, it is apparent that the various methods give a consistent and complementary description of the transitional behaviour under the given conditions of temperature and strain rate.

The brittle and ductile fracture regions of a mixed-mode fracture surface are shown at higher magnification in Fig. 8. In the brittle region, undeformed rubber particles about 1 μm in diameter emerge from the surface and circular depressions of the

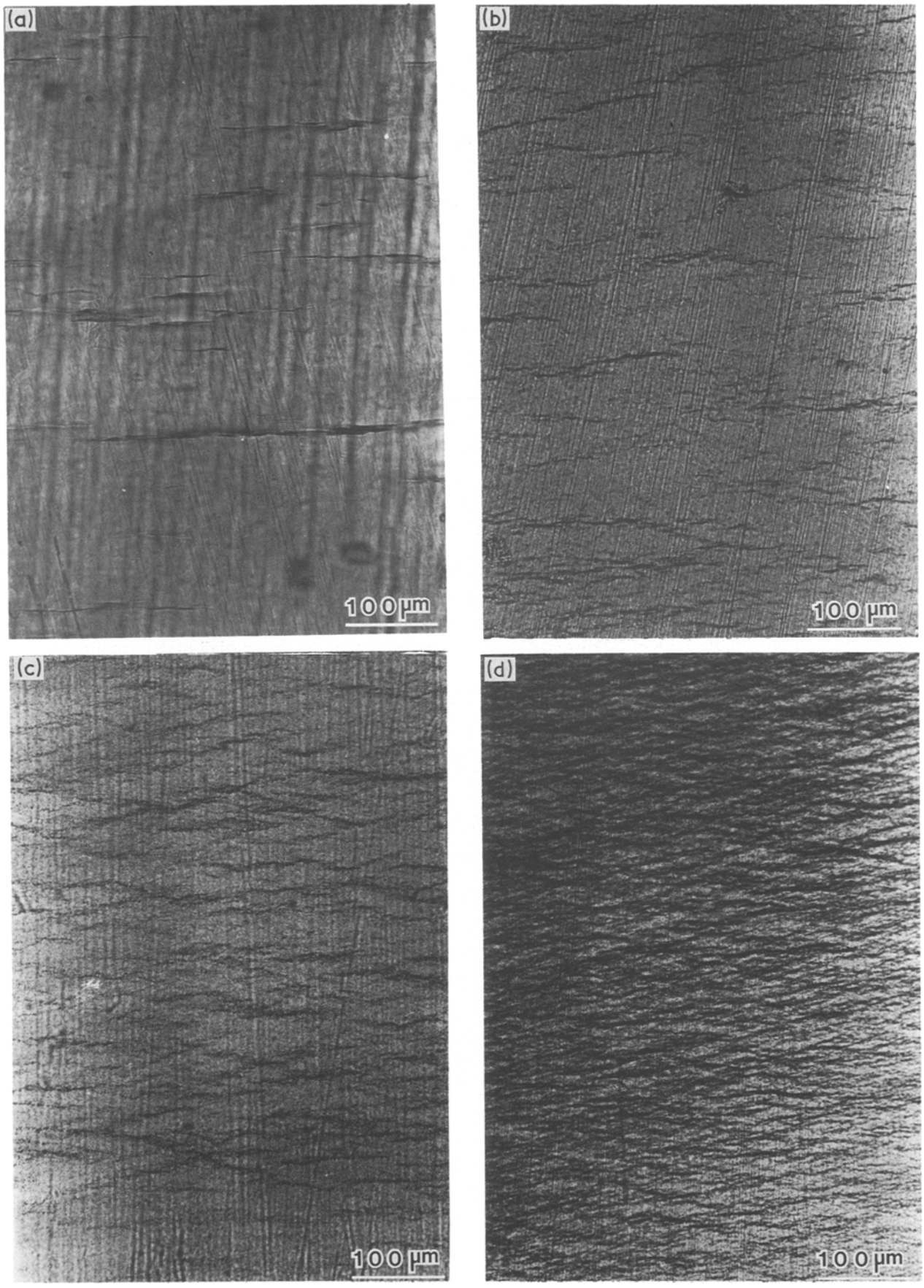

Figure 6 Fractured specimen viewed from the side close to the fracture site. The thin section is taken from the centre of the specimen. (a) PP, (b) 95% PP–5% EPR, (c) 90% PP–10% EPR, (d) 85% PP–15% EPR.

same size indicate where rubber particles previously resided. Furthermore there is no evidence of plastic deformation in the PP where the rubber particles separated from the matrix during brittle fracture. The ductile region of the fracture surface is characterized by extensive matrix flow and the appearance of large voids several times the diameter of the rubber particles. The localized plastic deformation of the matrix that occurs at stress concentrations caused by the rubber particles is a key to the enhanced macroscopic ductility of these and other blends [26–34].

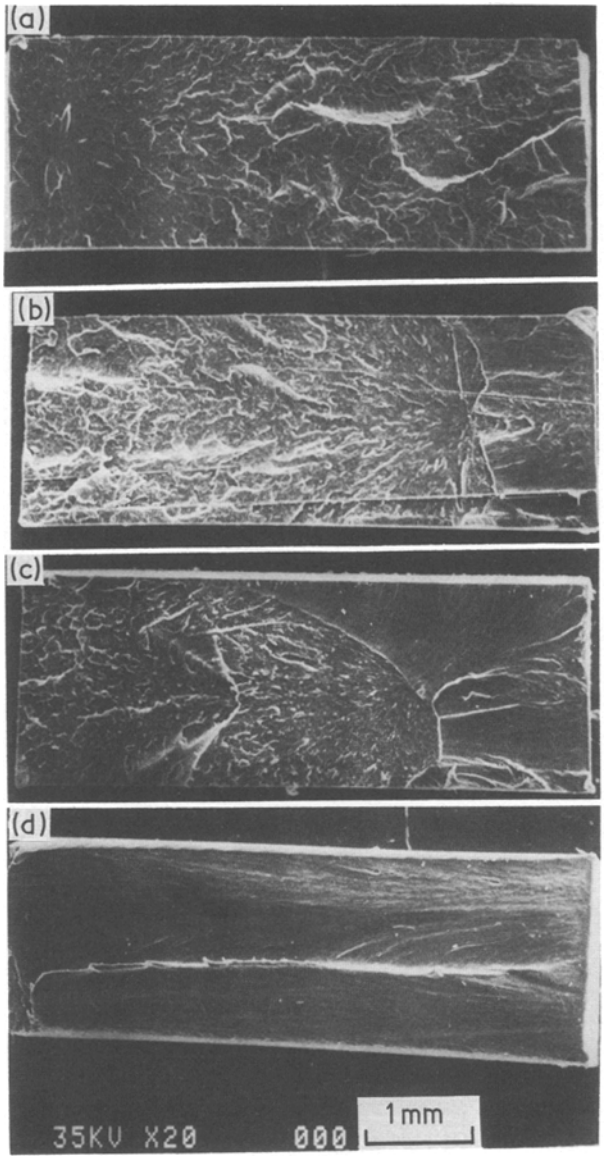

Figure 7 Scanning electron micrographs of fracture surfaces of (a) PP, (b) 95% PP–5% EPR, (c) 90% PP–10% EPR, (d) 85% PP–15% EPR.

3.3. Deformation at high strain rates

The ductile-to-brittle transition was also observed at ambient temperature when notched specimens were deformed in tension at high strain rates. The load–time curves for three ram speeds in Fig. 9 exhibit

TABLE IV Drop-dart impact strength

Sample PP (%)	Energy to break (J)
100	5.5
95	8.6
90	32.0
85	113.0
80	99.0
25	108.0

transitions with composition and strain rate. Two types of curve are observed, those where fracture occurs at the maximum stress and those that exhibit yielding where fracture occurs after the maximum in the load–time curve. At the highest ram speed, 450 in. min^{-1} (1143 cm min^{-1}), PP and the blends with 5 and 10% EPR fractured at the maximum stress. The increase in fracture stress with rubber content indicates that these specimens failed prematurely below the yield stress as is characteristic of brittle fracture. Based on the shape of the load–time curves, the ductile-to-brittle transition occurs between 15 and 10% EPR at the highest ram speed and coincides with an abrupt drop in the drop-dart impact strength (Table IV). The transition shifts to lower rubber content, between 10 and 5% and then between 5% and PP, as the ram speed decreases to 300 and 75 in. min^{-1} (762 and 191 cm min^{-1}), respectively.

The area under the load–time curve was divided at the maximum stress to obtain the elastic (A_1) and plastic (A_2) contributions to the fracture energy. The elastic component (Fig. 10) is not particularly sensitive to the speed but generally increases slightly with rubber content for both ductile fractures (solid symbols) and brittle fractures (open symbols). The plastic component with its strong dependence on rubber content is primarily responsible for a continuous increase in fracture energy with EPR content. The plastic component accounts for up to 70% of the total fracture energy in the most ductile specimens.

Longitudinal sections of the notched specimens fractured at 300 in. min^{-1} (762 cm min^{-1}) are shown in Fig. 11. In the side view of the PP specimen, only a clean fracture line is seen with no observable damage away from the fracture site. A small amount of craze-like damage is observed near the notch tip of the blend

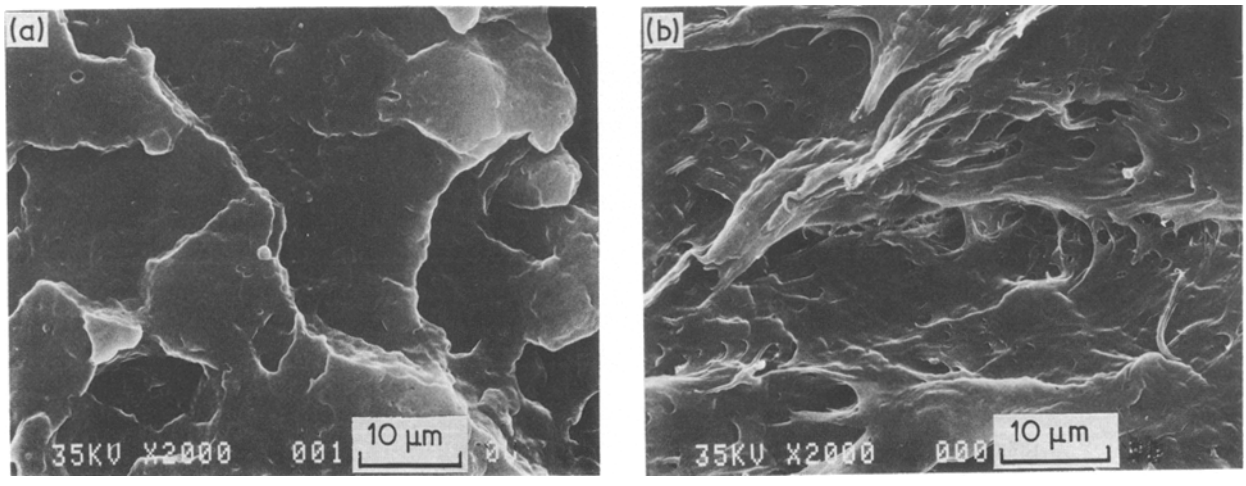

Figure 8 Higher magnification scanning electron micrograph of the fracture surface in Fig. 7b: (a) a region of brittle fracture, (b) a region of ductile fracture.

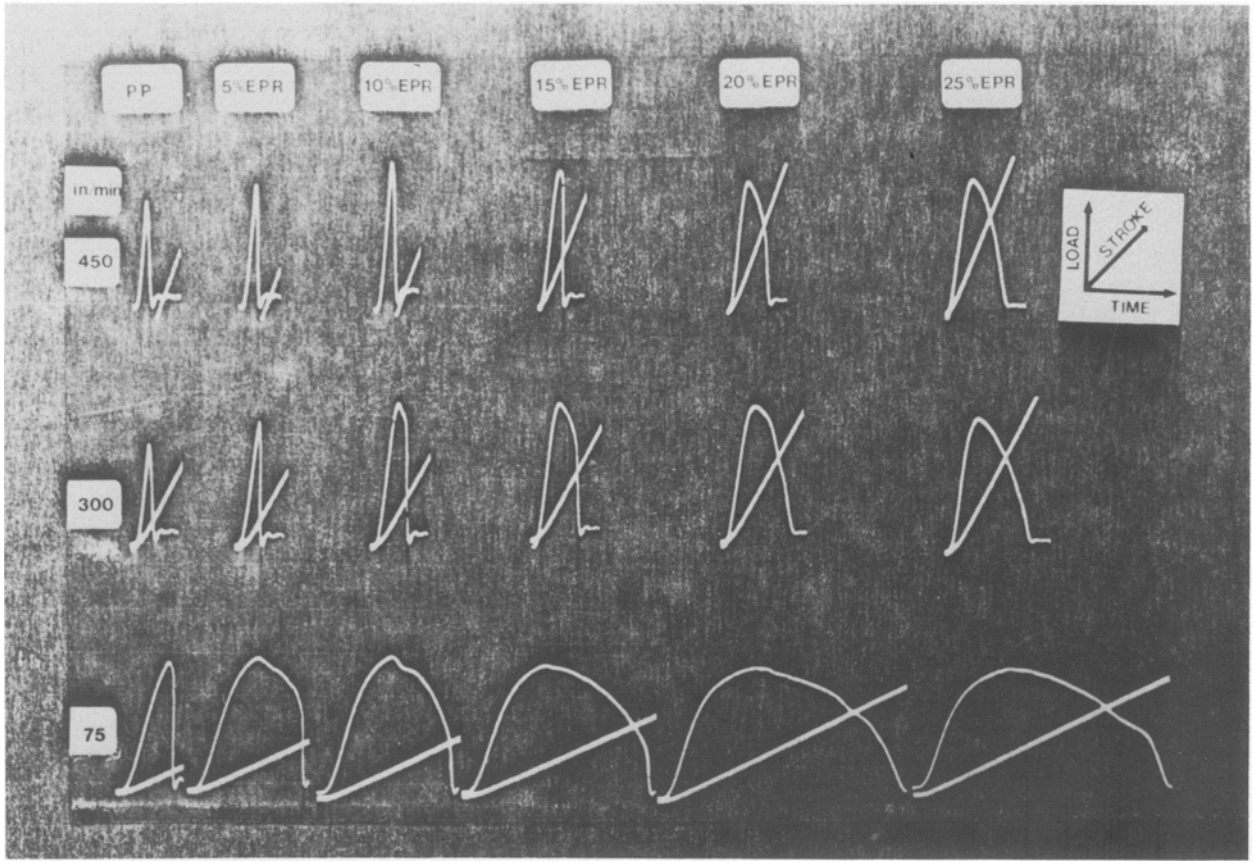

Figure 9 Load–time curves of notched specimens of PP blends at various ram speeds at room temperature. 1 in. = 2.54 cm.

with 5% EPR. In addition, a darkened region where voiding has occurred surrounds the craze-like damage and extends some distance away from the fracture surface. Although this specimen appeared from the macroscopic load–time curve to fracture in a brittle manner, the microscopic examination shows it has undergone a small amount of plastic deformation. Compared to the 5% EPR blend, a larger area of craze-like damage extends further across the 10% EPR specimen and the surrounding void region is also larger and more densely voided. In the 15% EPR blend the intense damage zone is even larger, and close to the fracture site crazes intersect to form crossing deformation bands similar to those observed in ductile specimens at low temperatures (cf. Fig. 6d). The amount of plastic deformation represented by the damage zones seen at the microscopic level is detected macroscopically as a gradual increase in the plastic contribution to the fracture energy A_2 with increasing EPR in the blend.

When fracture surfaces of the same notched specimens were examined in the SEM, that of PP was completely brittle, the fracture surface of the blend with 5% EPR was predominantly brittle with a small area of ductile fracture close to the notch, while a third of the surface nearest the notch was ductile in the 10% EPR blend. The fracture surface of the 15% EPR blend was entirely ductile. Brittle and ductile regions of the fracture surface of the 5% EPR are shown in Fig.12 before and after the rubber was removed by solvent etching. The undeformed particles in the brittle fracture surface far from the notch (Fig. 12a) are removed by solvent and only circular depressions of the same size are seen in the etched surface (Fig. 12b). The ductile fracture region close to the notch (Fig. 12c) shows large voids up to 10 μm in diameter that contain fibrillated material adhering to the sides. Voids in the etched surface are empty holes (Fig. 12d), indicating that the fibrillated material is rubber and failure occurred at the rubber–matrix interface. The interface does not fail completely and the micrograph in Fig. 12c provides evidence of adhesion between PP and EPR as predicted by the solubility parameters [8].

From the microscopic observations, plastic deformation of the notched specimens can be described by two zones (Fig. 13). Closest to the fracture site is an intense zone comprised of craze-like damage and, where the crazes are most dense, interaction and coalescence of crazes to form intersecting deformation bands. A second region characterized by profuse voiding extends over a much larger area well away from the fracture site.

The damage processes were examined at the microscopic level only in fractured specimens. Nevertheless, because the stress varies over the notched specimens, it is possible to correlate damage at different locations with the stress–strain relationship of the material. Initially, this is done qualitatively without actual calculation of the stress distribution. Observable damage furthest from the notch, which will be the initial irreversible deformation in the stress–strain curve, is voiding that follows failure of the rubber–matrix interface. Voiding extends over a large region of the specimen and is increasingly profuse, judging from the

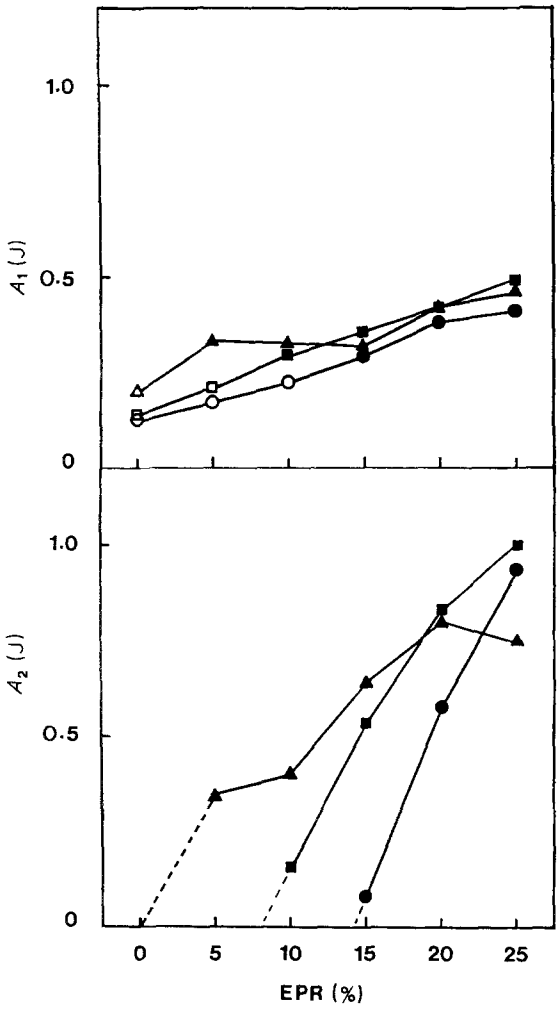

Figure 10 Fracture energy (single-edge notch, room temperature) of elastic deformation (A_1) and plastic deformation (A_2) as a function of composition at various ram speeds: (△, ▲) 75 in. min^{-1}, (□, ■) 300 in. min^{-1}, (○, ●) 450 in. min^{-1} (1 in. = 2.54 mm). Solid symbols, ductile fracture; open symbols, brittle fracture.

intensity of stress-whitening, as the rubber content increases.

Closer to the fracture site, where the specimen experiences higher stresses, the voids coalesce to form craze-like damage structures. There is a relatively clear demarcation between the voided region and the intense damage zone where crazing begins. Within the latter, interaction of the craze-like structures produces intersecting deformation bands close to the fracture site. Fracture occurs when the crack propagates through the intense damage zone. Increased proximity to the fracture site represents increasingly higher stresses on the stress–strain curve. When damage in the intense zone close to the fracture site is compared at the microscopic level with the fractured specimens from the low-temperature stress–strain measurements, it is seen that the same microdeformation mechanisms operate in the ductile-to-brittle transition region. These therefore represent unique phenomena that control the ductile-to-brittle transition in this system through their d pendence on composition and external variables of temperature and strain rate.

4. Conclusions

The nature of the ductile-to-brittle transition of PP–EPR blends has been related to the irreversible microdeformation processes that are responsible for mechanical energy absorption. In general, the ductile-to-brittle transition was dependent upon temperature, strain rate and composition. In unnotched specimens, the transition was studied in a temperature range below the glass transition temperature of PP where uniform deformation was observed. At room temperature, transitional behaviour was apparent at high strain rates with notched specimens where localized deformation ahead of the notch tip was observed. By examining the microdeformation mechanisms at the optical microscope level, the effects of composition were revealed. Specifically:

1. In unmodified PP, the controlling irreversible deformation process at $-40°$ C was crazing.
2. In the blends, two kinds of damage zone were observed: a diffuse zone due to voiding at the rubber particles, and an intense damage zone due to craze-like damage and deformation bands.
3. The ductile-to-brittle transition occurred gradually as a function of temperature or composition with a decrease in the size and density of both damage zones.

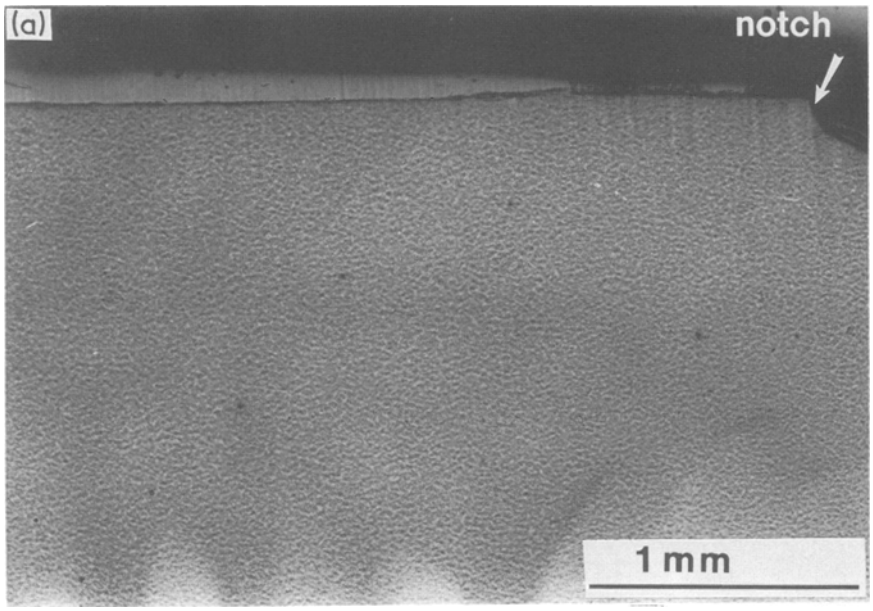

Figure 11 Optical micrographs of thin sections parallel to the applied stress direction: (a) PP, (b) 95% PP–5% EPR, (c) 90% PP–10% EPR, (d) 85% PP–15% EPR.

Figure 11 Continued.

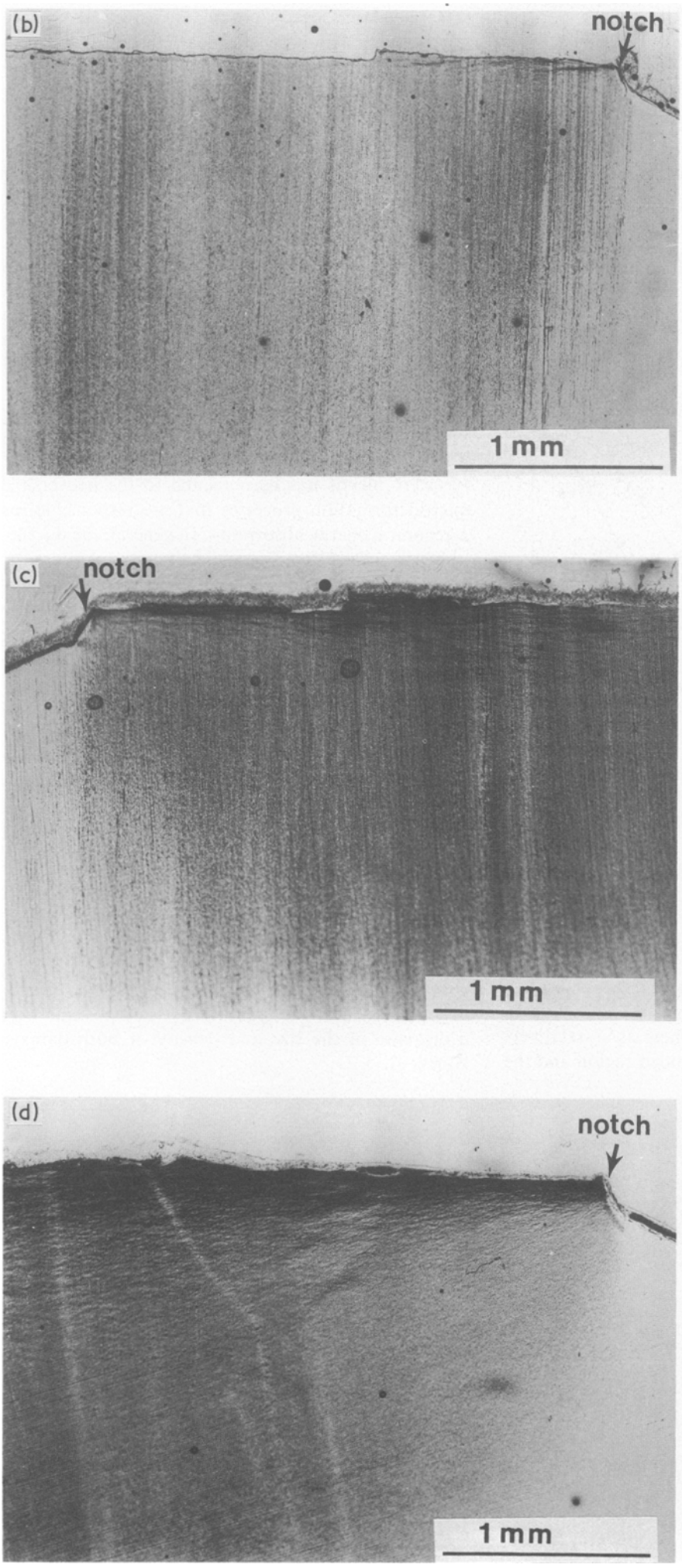

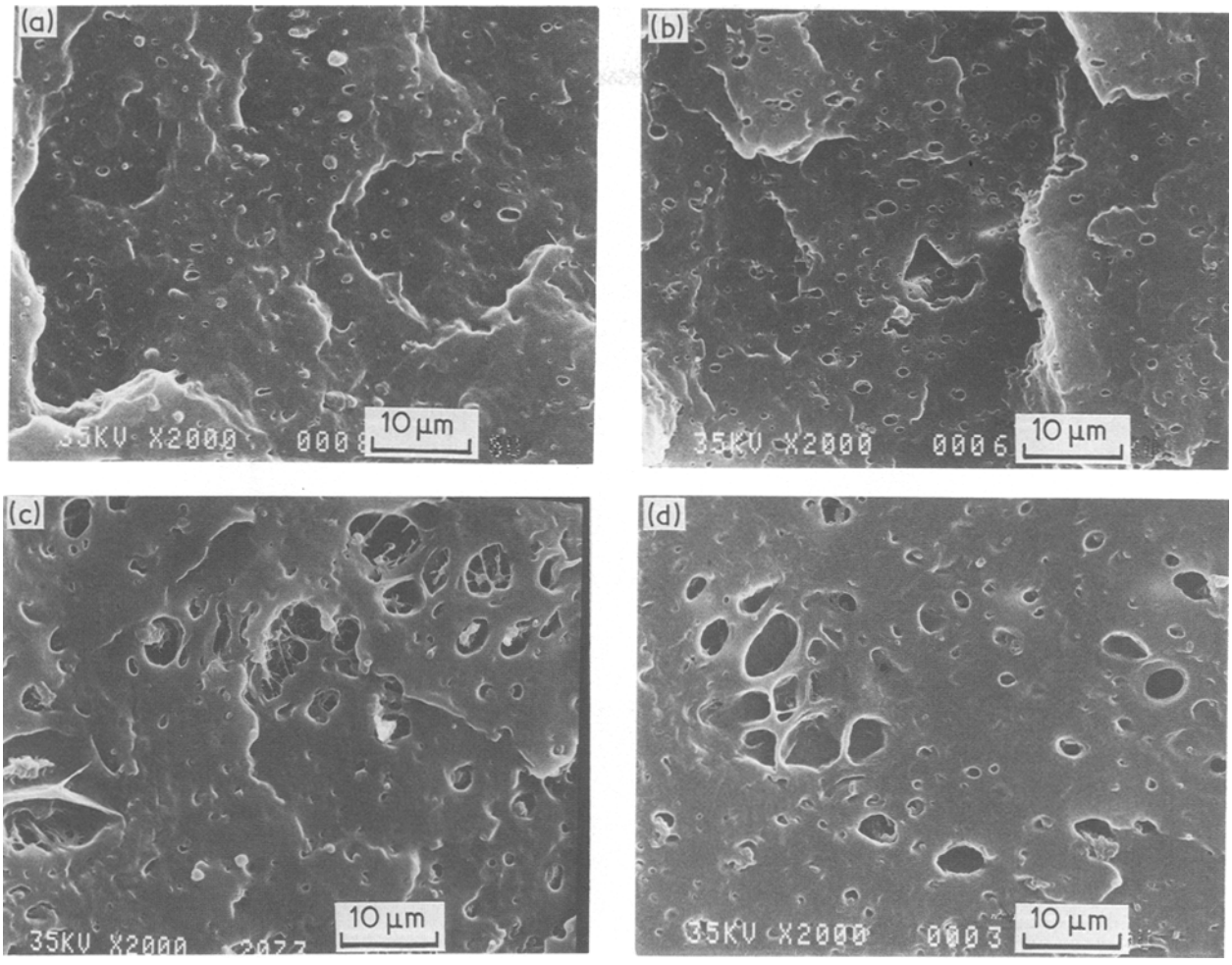

Figure 12 Scanning electron micrographs of the fracture surfaces of 95% PP–5% EPR at 300 in. min^{-1} (762 cm min^{-1}): (a) a region away from the notch, (b) etched surface at the same location as (a), (c) a region near the notch in the stress-whitening area, (d) etched surface at the same location as (c).

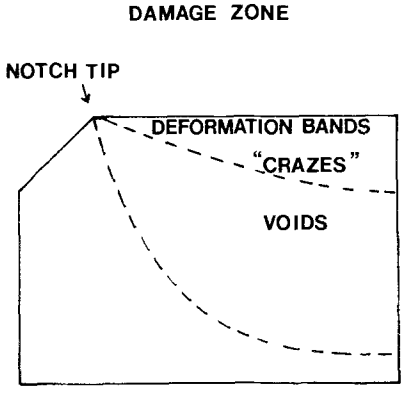

Figure 13 Schematic representation of the deformation zones observed ahead of the notch tip in PP blends.

Acknowledgement

This work was generously supported by the Whirlpool Corporation through the Center for Applied Polymer Research (CAPRI).

References

1. J. KARGER-KOCSIS, A. KALLO and V. N. KULEZNEV, *Polymer* **25** (1984) 279.
2. J. KARGER-KOCSIS, A. KALLO, A. SZAFNER, G. BODOR and Zs. SENYEI, *ibid.* **20** (1979) 37.
3. J. KARGER-KOCSIS, L. KISS and V. N. KULEZNEV, *Polym. Commun.* **25** (1984) 122.
4. E. MARTUSCELLI, C. SILVESTRE and G. ABATE, *Polymer* **23** (1982) 229.
5. Z. BARTCZAK, A. GALESKI and E. MARTUSCELLI, *Polym. Eng. Sci.* **24** (1984) 1155.
6. L. BIANCHI, S. CIMMINO, A. FORTE, R. GRECO, E. MARTUSCELLI, F. RIVA and C. J. SILVESTRE, *J. Mater. Sci.* **20** (1985) 895.
7. A. J. LOVINGER and M. L. WILLIAMS, *ibid.* **20** (1985) 895.
8. F. C. STEHLING, T. HUFF, C. S. SPEED and G. J. WISSLER, *J. Appl. Polym. Sci.* **26** (1981) 2693.
9. C. B. BUCKNALL, *Pure Appl. Chem.* **58** (1986) 986.
10. *Idem, ibid.* **58** (1986) 1000.
11. L. D'ORAZIO, R. GRECO, C. MANCARELLA, E. MARTUSCELLI, G. RAGOSTA and C. SILVESTRE, *Polym. Eng. Sci.* **22** (1982) 536.
12. J. KARGER-KOCSIS and V. N. KULEZNEV, *Polymer* **23** (1982) 699.
13. H. K. ASAR, M. B. RHODES and R. SALOVEY, in "Multiphase polymers", ACS Advances in Chemistry Series Vol. 176 (American Chemical Society, Washington DC, USA, 1979) p. 489.
14. F. COPPOLA, R. GRECO and G. J. RAGOSTA, *J. Mater. Sci.* **2** (1986) 1775.
15. D. YANG, B. ZHANG, Y. YANG, Z. FANG and G. SUN, *Polym. Eng. Sci.* **24** (1984) 612.
16. C. B. BUCKNALL, "Toughened Plastic" (Applied Science, London, 1977) p. 137.
17. S. NEWMAN, in "Polymer Blends", edited by D. R. Paul and S. Newman (Academic, New York, 1978) p. 63.
18. B. Z. JANG, D. R. UHLMANN and J. B. VANDER SANDE, *J. Appl. Polym. Sci.* **30** (1985) 2485.
19. *Idem, Polym. Eng. Sci.* **25** (1985) 643.
20. *Idem, J. Appl. Polym. Sci.* **29** (1984) 3409.

21. F. POLATO, G. PAGANETTO, M. BRAMUZZO and E. MARCHETTI, in the Proceedings of 6th International Conference on Deformation, Yielding and Fracture of Polymers, Cambridge, April 1985 (Rubber and Plastics Institute) p. 84.
22. C. B. BUCKNALL and C. J. PAGE, *J. Mater. Sci.* **17** (1982) 808.
23. "Polymer Handbook" (Wiley, New York, 1975) Ch. 111, p. 1.
24. K. FRIEDRICH, *Prog. Colloid Polym. Sci.* **66** (1979) 299.
25. B. Z. JANG, D. R. UHLMANN and J. B. VANDER SANDE, *Polym. Eng. Sci.* **25** (1985) 98.
26. A. F. YEE and R. A. PEARSON, *J. Mater. Sci.* **21** (1986) 2462.
27. R. A. PEARSON and A. F. YEE, *ibid.* **21** (1986) 2475.
28. M. A. MAXWELL and A. F. YEE, *Polym. Eng. Sci.* **21** (1981) 205.
29. A. F. YEE, *J. Mater. Sci.* **12** (1977) 757.
30. A. F. YEE, W. V. OLSZEWSKI and S. MILLER, in ACS Advances in Chemistry Series Vol. 154 (American Chemical Society, Washington DC, 1976) p. 97.
31. S. J. WU, *J. Polym. Sci., Polym. Phys. Edn* **21** (1983) 699.
32. *Idem. Polymer* **26** (1985) 1855.
33. T. KUNORI and P. H. GEIL, *J. Macromol. Sci.-Phys.* **B18** (1980) 93.
34. *Idem, ibid.* **B18** (1980) 135.

Received 21 July
and accepted 9 October 1987